

# RAINBOWS, HALOS, CORONAS AND GLORIES

## Beautiful Sources of Information

GUNTHER P. KÖNNEN

The study of rainbowlike features has seen a revival—relationships with properties of the scattering particles have been revisited, and the number of observations in other planetary atmospheres has increased.

If regularly shaped transparent particles of sufficient size are present in the atmosphere and if they are lit by the sun, colored structures may appear at specific locations on the celestial sphere. The best known among these structures is the primary rainbow, which appears in sunlit raindrops as a colored circular segment of radius  $42^\circ$ , centered on one's shadow point (also called the antisolar point). Almost equally well known is the lunar diffraction corona in its most basic form: a reddish circle a few degrees wide that surrounds the moon. Less known though more common than rainbows are halos, which appear in sunlit ice crystals and are chiefly located on the sun side of the celestial sphere. Even lesser known is the glory, which appears as a "minirainbow" around one's shadow when the shadow is cast on water clouds or fog. In past times it was rarely seen, but nowadays it is frequently seen by observant air travelers.

The opening statements of this article can equally well be formulated the other way around: if a halo or rainbow is observed in the sky, information is available about the shapes, sizes, and/or composition of airborne particles. Each phenomenon carries its own specific information about the particles that generate it. This information is sometimes difficult to obtain from other sources. The appearance of most of these phenomena is transient ▶

Detail of a secondary rainbow over Brannenburg, Germany. See Fig. 3 for the full image.



**FIG. 1. Primary and secondary rainbows in a rain shower over New Mexico (NM). The color sequence of the bows is reversed; the sky is darkest between the bows. The reversed colors of the secondary rainbow arise because the emerging light rays cross the incoming light rays. Because of the flattened shape of the falling drops, the primary rainbow is slightly flattened in heavy showers. The diagrams (labeled 1 and 2) indicate the ray paths through the drop that form the primary and secondary rainbows. Photograph taken by H. E. Edens in Magdalena, NM, at 2336 UTC 22 Sep 2013. Solar elevation is 17.6°.**

and occurs at unpredictable times. But in cases where the actual state of the atmosphere at a certain moment is of importance, or when one is interested in knowing the composition of particles floating in the air, their observation may help.

This paper describes the appearance and peculiarities of these four phenomena, the information they contain, new insights that have been gained during the past 40 years, and cases where they have been observed from space in the atmospheres of planets.

**RAINBOWS AND THEIR INFORMATION CONTENT.** “Normal” rainbows and their super-numeraries. The chief characteristic of a rainbow is its roundness, which is a direct consequence of the sphericity of drops. So the presence of a rainbow tells us that there are spherical particles present in the sky: water drops, of course. When a drop is flattened, its primary rainbow is flattened as well (Venturi 1814; Brandes 1816; Möbius 1910). Large falling drops are flattened by aerodynamic forces and as a result so is the rainbow in heavy showers. For a low-sun rainbow, its distance to the antisolar point is about 1° smaller at its top than at its sides (Fraser 1983; Hausmann 2015).

The primary rainbow is generated by a light path through a drop that consists of entry–reflection–exit. An additional internal reflection creates another rainbow, called the secondary rainbow. That rainbow appears a few degrees outside the primary one and is recognizable by its reversed color sequence (Fig. 1). The 8°-wide region between the two rainbows is the darkest part of the sky. The secondary rainbow always accompanies the 8-times-brighter primary one, but because of its intrinsic dimness it often remains unnoticed.

The primary and secondary rainbows contain much the same physical information. A difference is that the secondary rainbow is always perfect circular, as its position in the sky is insensitive to the flattening that occurs for large falling drops (Können 1987). Thus, in contrast to the primary rainbow, the position of the top of the secondary rainbow contains no information about the nonsphericity of falling drops.

The internal reflections in the rainbow-making light paths through the drops happen to occur so close to the Brewster angle that rainbows are almost entirely polarized, which can be easily checked using a simple polarizer. If an isolated colored spot appears in the sky, rotating a polarizer in front of the eye can confirm whether the spot is a segment of a rainbow: when it disappears at a certain orientation of the polarizer, the identification is positive, and it is confirmed that the scatterers are drops.

The rainbow polarization is so strong that weak rainbows are more easily detected by their polarization rather than by their intensity. This is particularly useful if one tries to detect rainbows due to drops of sizes in the 10- $\mu\text{m}$  range and below, where the rainbow has lost its brilliance and has turned into a colorless white band. Such drops are usually the constituents of altocumulus clouds. If sunlit, they produce a

**AFFILIATION:** KÖNNEN\*—Royal Netherlands Meteorological Institute, De Bilt, Netherlands

\* Retired

**CORRESPONDING AUTHOR E-MAIL:** Gunther P. Können, [konnen@planet.nl](mailto:konnen@planet.nl)

The abstract for this article can be found in this issue, following the table of contents.

DOI:10.1175/BAMS-D-16-0014.1

In final form 8 August 2016  
©2017 American Meteorological Society

white rainbow at  $\sim 35^\circ$  from the shadow point, but this inconspicuous bow is often lost in the chaotic structure of the cloud elements. However, with a polarizer the rainbow component in the cloud's radiance appears clearly. In this way, rainbows can be seen on almost every partly cloudy day, albeit only with a polarizer (Können 1985).

The rainbow angle depends on the refractive index and hence on the chemical composition of the drops. Seawater, having a higher refractive index than freshwater, shifts the rainbow in the direction of the antisolar point. Scrutinizing the rainbow shift in Fig. 2 as a function of wavelength could reveal that seawater contains salt (NaCl). Obviously, there exists a more direct method to find out that seawater is salty. But for planets other than Earth it is not so easy. In the early 1970s Hansen and Hovenier (1974) recognized a prominent rainbow peak in the polarization of Venus and analyzed its properties and its shift relative to a freshwater rainbow. From this they concluded that the Venus upper clouds consist of drops with sizes on the order of microns, and that these drops would taste somewhat sour rather than salty because they very likely consist of concentrated sulfuric acid. In the late 1970s this conclusion was beautifully confirmed by in situ measurements of descending space probes.

Not every rainbow feature offers the information it suggests. A deceptive example comes from the narrow bows visible close to the inside of the primary rainbow, called the supernumerary bows (Fig. 3), which are caused by the interference of rays inside the droplet.



**FIG. 2.** The rainbow in freshwater raindrops is extended below the horizon by a rainbow in seawater spray. The slightly larger refractive index of saltwater drops causes the radius of the subhorizon rainbow to be  $0.8^\circ$  less than that of the above-horizon freshwater rainbow. Photograph taken by J. Dijkema in the Pacific Ocean, 800 km southeast of Japan, during 1981. Solar elevation is  $32.5^\circ$ .



**FIG. 3.** Primary rainbow with two interference bows along its inner side (the supernumerary bows). An incorrect conclusion may be drawn from the spacing between the interference bows if the rainbow appears in a heavy shower. Their spacing does relate to the size of the rainbow-generating drops, but in the case of a broad drop size distribution (such as in the case of heavy showers), the size of the rainbow-generating drops is not related to the mean drop size in the shower. Photograph taken by C. Hinz in Brannenburg, Germany, at 1424 UTC 21 Aug 2009. Solar elevation is  $36.9^\circ$ .

The obvious explanation is that the spacing between the bows relates to the droplet size in rain. For a peaked drop size distribution this is indeed the case,

but for a broad and flat drop size distribution, as occurs in heavy showers, it is not. In fact, because of smearing one would expect no interference fringes at all. As pointed out by Fraser (1983), supernumeraries nevertheless arise in this case because of the shift of the rainbow angle as a result of the flattening of falling drops. This causes a selection effect that for any broad drop size distribution produces

supernumeraries with mutual spacing of about  $0.7^\circ$  (corresponding to a drop diameter of 0.5 mm), but the spacing between these interference bows does not contain any useful information about the range of drop sizes in the shower.

*High-order rainbows: Seen in nature, at long last.* Light that has undergone three internal reflections during

its path through a drop makes a third rainbow, four reflections a fourth rainbow, and so on. These “high-order rainbows” become increasingly weaker. Just like the primary and secondary rainbows, the third and fourth rainbows are close together (separated by about  $6^\circ$ ) and have their red sides facing each other. However, this duo appears on the bright side of the sky,  $45^\circ$  from the sun. The fifth rainbow is located in the region opposite the sun again, not far from the primary and secondary rainbows.

Although there are no *a priori* reasons that prevent the observation of the third rainbow in nature, it was only recently that it was unambiguously detected. Before 1700 it was searched for in the wrong part of the sky (Boyer 1987), and since then only a handful of possible sightings of the third rainbow have been reported, most of them being



**FIG. 4.** First picture ever of the fourth rainbow and second picture ever of the third rainbow. This pair of high-order rainbows appears on the sun side of the sky and is made visible by contrast enhancement; the foreground landscape is not contrast enhanced. As in the case of the primary and secondary rainbows, the third and fourth rainbows have their red sides toward each other. However, the spacing between them is decreased. The diagrams (labeled 3 and 4) indicate the ray paths through the drop that form the third and fourth rainbows. Photograph taken by M. Theusner in Schiffdorf, Germany, at 1819 UTC 11 Jun 2011. Solar elevation is  $10.9^\circ$ .



**FIG. 5.** First picture ever of the fifth rainbow. The green and blue hues between the primary and secondary rainbows are from the (broad) fifth rainbow whose red component is hidden by the much brighter secondary rainbow. The picture is contrast enhanced. The diagrams (labeled 1, 2, and 5) indicate the ray paths through the drop that form the primary, secondary, and fifth rainbows. Photograph taken by H. E. Edens at Langmuir Laboratory, NM, at 2350 UTC 8 Aug 2012. Solar elevation is  $26.4^\circ$ .

of dubious quality (Lee and Laven 2011). This changed dramatically in 2011 when Großmann (2011), inspired by the above study by Lee and Laven, decided to take “in the blind” pictures in the correct direction, and after some image processing, the long-searched-for third rainbow was found! One month later, in an attempt to reproduce this successful observation, Theusner (2011) obtained a picture containing both the third and fourth rainbows. In 2012 Edens (2015) photographed the fifth, and in 2014 he found traces in his earlier pictures of what could be the seventh rainbow (Edens and Können 2015). Since then, more pictures of high-order rainbows have become known. Figure 4 shows the iconic picture of the third and fourth rainbows by Theusner; Fig. 5 shows the discovery picture with the green and blue hues of the fifth rainbow—its red being hidden behind the much brighter secondary rainbow.

### ATMOSPHERIC HALOS AND THEIR INFORMATION CONTENT.

Halos not only exist in the form of colored circles around the sun, but can also appear as arcs, spots, streaks, loops, and circles at various locations of the celestial sphere, a consequence of the faceted nature of crystals. Simple isolated halos occur frequently in the sky: in the midlatitudes, a well-trained observer may see a halo or a trace of it typically five to seven times per month (Minnaert 1993), but for others often halos remain unnoticed because of their proximity to the sun. Sunglasses help to improve one’s observational record.

The presence of halos indicates that polyhedral solid particles are present in the atmosphere, namely ice crystals. Any pair of crystal faces may act as a refracting prism, generating colored phenomena concentrated on the sun side of the sky. If the crystals are randomly oriented, the halos appear as concentric circles centered on the sun, with radii depending on the refractive index and the angle between the refracting faces. However, usually many of the halo-making crystals assume a

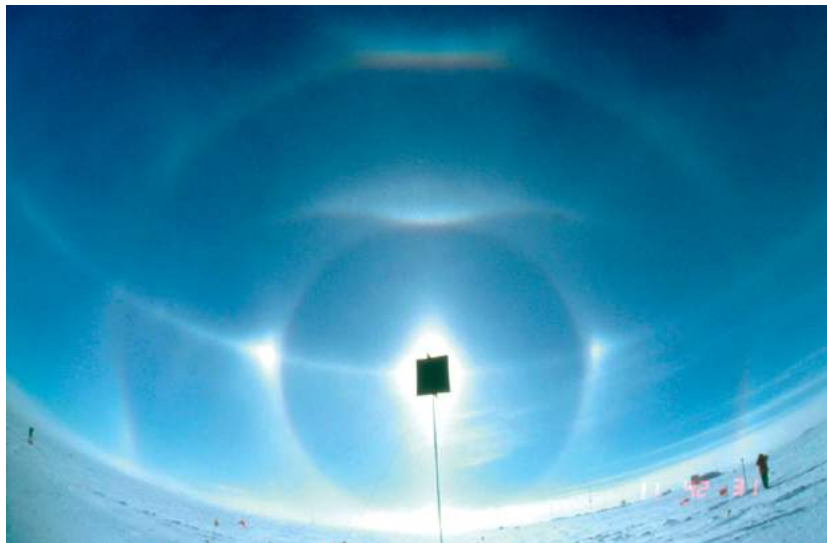


**Fig. 6. Complex halo display due to simple ice crystals. This rich halo display is due to simple hexagonal ice crystals with flat ends, floating in various modes of orientation. The two circular halos are due to crystals having random orientations and have radii of  $22^\circ$  and  $46^\circ$ , respectively. Associated with these circular halos are arcs caused by the same crystals in the swarm, but now preferentially oriented. The spots to the right and left of the sun are the  $22^\circ$  parhelia (“sundogs”). The names of the many other halo arcs can be found in Tape (1994). The sixfold symmetry in the arrangement of the arcs associated with the  $46^\circ$  halo is an expression of the sixfold symmetry of the ice crystals causing the display. The sun is hidden behind a nearby object. This display is outstanding; more frequent mediocre displays are bleaker and usually lack the  $46^\circ$  features. Photograph taken by G. P. Können at U.S. Amundsen–Scott South Pole Station ( $90^\circ\text{S}$ ) at 2243 UTC 1 Jan 1998. Solar elevation is  $23.0^\circ$ . The horizontal field of view is  $135^\circ$ .**

preferential orientation in the air, which results in the appearance of a large variety of colored or white halo structures—many of them being positioned near the circular halo to which they are associated and others occurring at other locations on the celestial sphere (Greenler 1989; Tape 1994; Tape and Moilanen 2006).

Mostly, halo-making ice crystals are hexagonal plates or columns with flat ends. The two possible refracting prisms in these simple crystals have interfacial angles of  $60^\circ$  and  $90^\circ$ , giving rise to halos grouped at  $22^\circ$  and  $46^\circ$  from the sun, respectively. Figure 6 shows a well-developed halo display with circular halos as well as halo arcs. The arrangement of the halo arcs around the circular halos is not random but represents a mapping of the crystal symmetry onto the celestial sphere; for example, the sixfold symmetry in the arrangement of the arcs associated with the  $46^\circ$  circular halo in Fig. 6 is an expression of the sixfold symmetry of ice crystals. Sometimes terrestrial halos originate from ice crystals with pyramidal instead of flat faces at their ends (Tape and Moilanen 2006; Tape 1994 and references therein), which results in a different and often



**FIG. 7. Complex halo display due to exotic ice crystals. This halo display is caused by hexagonal ice crystals having pyramidal rather than flat ends. The presence of these crystals manifests itself by the appearance of multiple circular halos with radii between  $18^\circ$  and  $24^\circ$ , the vanishing of most of the  $22^\circ$  and  $46^\circ$  features in Fig. 6, and the appearance of strange-shaped halo arcs at unusual places. The sun is hidden behind a nearby object. This stacked picture is contrast enhanced. Photograph taken by M. Riikonen at Oulu, Finland, around noon on 17 Sep 2001. Solar elevation is  $27^\circ$ . The horizontal field of view is  $135^\circ$ .**



**FIG. 8. (left) Halo in the terrestrial atmosphere. (right) Halo in the thin clouds of Mars. The white streak in the pictures is the so-called subsun, a halo that appears as an elongated mirror image of the sun in the clouds. It is due to the reflection of sunlight by horizontally oriented crystal faces; see the diagram in the left panel. The picture of the terrestrial subsun is taken from an aircraft; its length ( $\sim 4^\circ$ ) indicates a mean tilt angle of  $1^\circ$  of the reflecting crystal faces. The Mars picture is taken by a scanning platform, causing the Martian subsun to be strongly elongated. Left photograph taken by M. Vollmer on a flight from Fairbanks, AK, to Frankfurt, Germany, at 0238 UTC 9 Aug 2013. Solar elevation is  $\sim 10^\circ$ . The horizontal field of view is  $16^\circ$ . Right photograph taken on 28 Jan 2006 by the National Aeronautics and Space Administration/Jet Propulsion Laboratory/Malin Space Science Systems (NASA/JPL/MSSS) Mars Orbiter Camera (MOC2-1363), covering an area of  $1800 \text{ km} \times 2400 \text{ km}$  on Mars.**

more complicated halo display (Fig. 7). To many people, the shapes of crystals bear a certain beauty. Great halo displays are celestial manifestations of this crystalline beauty.

Halos contain information about the interfacial angles within a crystal, the refractive index and hence the chemical composition of the solid, the crystal symmetry, the shape of the crystals, and the orientation that falling crystals assume in the air. From the features appearing in a halo display a model of the halo-making crystals can be constructed. The richer the halo display, the more unique is the reconstruction. Although the terrestrial halo makers are nowadays well understood, surprises sometime occur. In 1997 the appearance of an

atypical halo display (Riikonen et al. 2000) proved the presence in the atmosphere of preferentially oriented ice crystals with exotic pyramidal faces—a type of ice crystal that had not been detected before in the free atmosphere (Lefaudeux 2011).

Halos are expected to occur in the atmospheres of other planets as well. A bright subhorizon halo streak has indeed been observed on Mars by an orbiting space probe (Fig. 8), but that type of halo is due to external reflection at the crystal faces, and thus contains only information about the degree of preferential orientation of the halo-generating airborne Martian crystals, not about the composition of these crystals (Können 2006). In 2005, during the descent of the *Huygens* probe through the dense atmosphere of Saturn's moon Titan, we were eager to look for halos from methane crystals (Können 2004), but nothing showed up in the images. In fact, at a height of 21 km above the surface, the probe passed through a swarm of particles that were most likely methane crystals (Tomasko et al. 2005), but at that stage of the descent, the sky above the probe was overcast. Hopefully, on another occasion the Titan weather will be more cooperative.

#### **DIFFRACTION CORONAS AND GLORIES, AND THEIR INFORMATION CONTENT.**

*Diffraction coronas.* The diffraction corona, not to be mistaken for the much larger halos, consists in its



**FIG. 9. Typical diffraction corona around a gibbous moon, during morning twilight. In the naïve and widely applied approach, the angular diameter of the red ring, about  $1.7^\circ$ , which surrounds the white aureole, indicates a particle size of  $35 \mu\text{m}$ . This turns out to be an overestimation by almost a factor of 2. Photograph taken by C. Hinz from the mountain Wendelstein (1835 m) in the Bavarian Alps at 0636 UTC, 15 min before sunrise, on 22 Jan 2011. Solar elevation is  $-3.0^\circ$ . The horizontal field of view is  $10^\circ$ .**

simplest form of a white aureole, with angular diameter of a few degrees, surrounding a light source and terminating in a reddish outer edge (Fig. 9). Sometimes it is surrounded by additional colored rings. The diffraction corona occurs a couple of times during virtually every partially clouded day. Many people are familiar with the diffraction corona surrounding the moon but are unaware of its brilliant counterpart surrounding the sun, as one instinctively avoids looking in the close vicinity of the sun. However, with the aid of sunglasses and by blocking the solar disk with one's thumb, one can see the fine color hues of the sunlight-induced diffraction corona in their full richness.

The corona is caused by diffraction of light by micron-sized cloud particles, in most cases water drops. As is the case for rainbows, the roundness of the diffraction corona is an expression of the sphericity of the drops. The diameter of the diffraction corona is inversely proportional to the drop size. Hence, the corona expands where it extends over the smaller drops at the edge of a cloud. Intrinsic noncircular coronas exist, occasionally with a marked internal structure (Evans 1913; Corliss 1977; Parviainen et al. 1994), but these small-sized phenomena are caused by oriented pollen instead of by deformed drops (Tränkle and Mielke 1994).

Quantitative values of the drop size can be directly inferred from the diameter of the diffraction corona.

This has been frequently done using the diameter of the red ring surrounding the bright central aureole (seen in Fig. 9). However, as recently pointed out by Laven

(2015), this ring is not the first diffraction maximum, but instead is the result of the wavelength dependence of the width of the central aureole. Therefore the often-applied and seemingly obvious use of Fraunhofer diffraction theory to the inner red ring is incorrect and results in an overestimation of the particle sizes by no less than a factor of 2. It is fascinating that this mistake has remained unnoticed by many for nearly two centuries.



**FIG. 10.** Typical appearance of a glory as seen from an aircraft. The glory is centered on the shadow of the plane or, better, on the shadow of the camera that took this picture. The distance of the glory's center below the horizon indicates a solar elevation of  $13.5^\circ$ . The angular diameter of the glory's inner red ring of about  $8^\circ$  indicates a drop diameter of about  $10\ \mu\text{m}$ . Photograph taken by P. Laven at 1649 UTC 30 Mar 2005, shortly after takeoff on a flight from Geneva, Switzerland, to London, United Kingdom. The horizontal field of view is  $50^\circ$ .



**FIG. 11.** Deformed glory on a cap cloud over the top of a neighboring mountain. The gradients in droplet size cause the formation of a colored sideward extension on the right-hand side of the glory. A detailed analysis reveals drop diameters ranging from about  $35\ \mu\text{m}$  in the undisturbed part down to  $15\ \mu\text{m}$  in the colored extension (Laven 2008b). The picture is contrast enhanced. Photograph taken by C. Hinz from the mountain Wendelstein (1835 m) in the Bavarian Alps at 0726 UTC 18 Nov 2007. Solar elevation is  $8.3^\circ$ . The horizontal field of view is  $13^\circ$ .

*Glories.* The corona has its counterpart on the opposite side of the celestial sphere. This phenomenon is called the anticorona or the glory. Its shape resembles the diffraction corona, consisting of a white central area with angular diameter of a few degrees surrounded by a reddish ring, but now the center is at the shadow point (Fig. 10). Sometimes a second or even a third concentric ring is present.

The glory is caused by backscattering of light by small drops via a mechanism different than that of the diffraction corona. Given the many sightings reported by pilots, it is probably as common as the diffraction corona, but ground-based observers rarely see it.

The diameter of the glory is inversely proportional to the drop size. Noncircular glories regularly occur, but they are the result of gradients in the droplet sizes in the cloud deck where the glory appears, rather than being an indication of nonsphericity of the tiny drops (Fig. 11).

The presence of a glory implies that spherical particles of a certain size are present at the site of its appearance. These spheres have to be transparent in order to create a glory, but somewhat counterintuitively, the structure and diameter of a glory does not contain any useful information about the refractive index, and hence about the chemical composition, of the

glory-making particles (Laven 2008a).

The mechanism causing the glory had remained a mystery for a long time: it was only in 1947 that Van de Hulst formulated the first reasonable model of the formation of this enigmatic phenomenon (Van de Hulst 1947). However, it took another half century until the glory was fully understood (Laven 2005b)—a clear illustration of the fact that the development and evolution of atmospheric optics is still in progress.

Glories in the terrestrial atmosphere have been observed from space (Floor 2012; Israelevich et al. 2009; see Fig. 12) and recently also in the atmosphere of Venus (Markiewicz et al. 2014; Petrova et al. 2015). As our exploration of the solar system is still at its very early stage and research on exoplanets is booming, the detection of glories, halos, or rainbows in the atmospheres of planets other than Earth, Venus, or Mars, or even perhaps in the atmosphere of an Earth-like exoplanet (Karalidi et al. 2012), seems to be just a matter of time.

**POSTSCRIPT.** Many aspects of the development in the field in the past 40 years are condensed in the special issues on Light and Color in the Open Air that have appeared since 1979 every 3–4 years in the Optical Society of America (OSA) publications *Journal of the Optical Society of America* (1979–1987) and *Applied Optics* (1991–2015). See Shaw et al. (2015) for a complete listing of these special issues.

## REFERENCES

- Boyer, C. B., 1987: *The Rainbow: From Myth to Mathematics*. Princeton University Press, 376 pp.
- Brandes, H. W., 1816: Venturi's Theorie des farbigen Bogens, welcher sich oft an der innern Seite des Regenboges zeigt, dargestellt mit einigen Anmerkungen. *Ann. Phys.*, **52**, 385–397, doi:10.1002/andp.18160520404.
- Corliss, W. R., 1977: *Handbook of Unusual Natural Phenomena*. Sourcebook Project, 542 pp.
- Edens, H. E., 2015: Photographic observation of a natural fifth-order rainbow. *Appl. Opt.*, **54**, B26–B34, doi:10.1364/AO.54.000B26.
- , and G. P. Können, 2015: Probable photographic detection of the natural seventh-order rainbow. *Appl. Opt.*, **54**, B93–B96, doi:10.1364/AO.54.000B93.
- Evans, L., 1913: Remarkable lunar halo. *Quart. J. Roy. Meteor. Soc.*, **39**, 154, doi:10.1002/qj.49703916609.
- Floor, C., 2012: Glory from space. *Weather*, **67**, 41, doi:10.1002/wea.868.
- Fraser, A. B., 1983: Why can the supernumerary bows be seen in a rain shower? *J. Opt. Soc. Amer.*, **73**, 1626–1628, doi:10.1364/JOSA.73.001626.
- Greenler, R., 1989: *Rainbows, Halos, and Glories*. Cambridge University Press, 195 pp.
- Großmann, M., E. Schmidt, and A. Haußmann, 2011: Photographic evidence for the third-order rainbow. *Appl. Opt.*, **50**, F134–F141, doi:10.1364/AO.50.00F134.
- Hansen, J. E., and J. Hovenier, 1974: Interpretation of the polarization of Venus. *J. Atmos. Sci.*, **31**, 1137–1160, doi:10.1175/1520-0469(1974)031<1137:IOTPOV>2.CO;2.
- Haußmann, A., 2015: Observation, analysis, and reconstruction of a twinned rainbow. *Appl. Opt.*, **54**, B117–B127, doi:10.1364/AO.54.00B117.

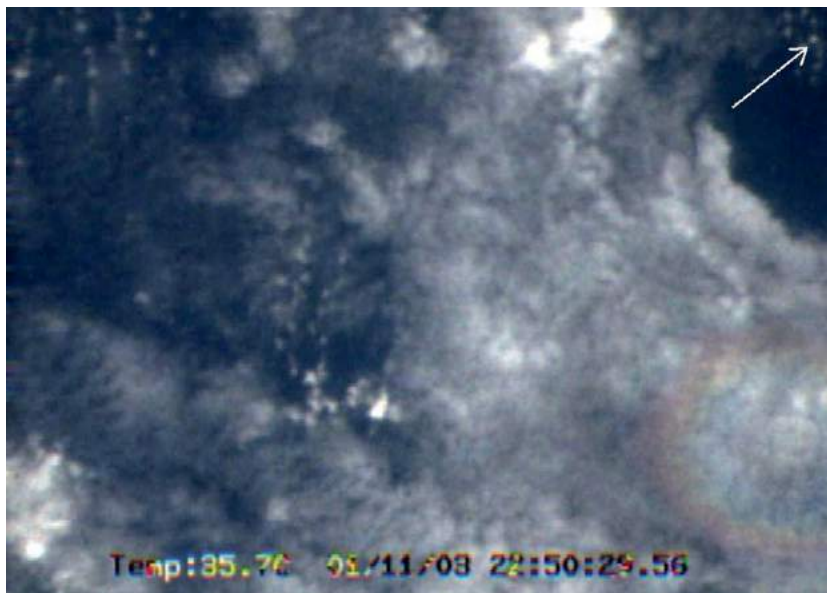


**FIG. 12. Glory observed from space. The angular diameter of the glory of about  $3^\circ$  corresponds to a drop diameter of about  $30 \mu\text{m}$  (Laven 2005a). Photograph taken above the Atlantic by the Israeli astronaut I. Ramon, on board the ill-fated space shuttle *Columbia*, at 1429:30 UTC 28 Jan 2003, 4 days before the crash. The glory's center is at  $0.7^\circ\text{S}$ ,  $12.7^\circ\text{W}$ , 750 km southwest of Liberia. The horizontal field of view of  $14.0^\circ$  covers 77 km on Earth's surface. The arrow indicates north. (Image reproduced with permission of P. Israelevich, Tel Aviv University, Tel Aviv, Israel.)**

- Israelevich, P. L., J. H. Joseph, Z. Levin, and Y. Yair, 2009: First observation of glory from space. *Bull. Amer. Meteor. Soc.*, **90**, 1772–1774, doi:10.1175/2009BAMS2824.1.
- Karalidi, T., D. M. Stam, and J. W. Hovenier, 2012: Looking for the rainbow on exoplanets covered by liquid and icy water clouds. *Astron. Astrophys.*, **548**, A90, doi:10.1051/0004-6361/201220245.
- Können, G. P., 1985: *Polarized Light in Nature*. Cambridge University Press, 172 pp.
- , 1987: Appearance of supernumeraries of the secondary rainbow in rain showers. *J. Opt. Soc. Amer.*, **4A**, 810–816, doi:10.1364/JOSAA.4.000810.
- , 2004: Titan halos. *Titan, From Discovery to Encounter*, K. Fletcher, Ed., ESA SP-1278, 323–330.
- , 2006: A halo on Mars. *Weather*, **61**, 171–172, doi:10.1256/wea.46.06.
- Laven, P., 2005a: Atmospheric glories: Simulations and observations. *Appl. Opt.*, **44**, 5667–5675, doi:10.1364/AO.44.005667.
- , 2005b: How are glories formed? *Appl. Opt.*, **44**, 5675–5683, doi:10.1364/AO.44.005675.
- , 2008a: Effects of refractive index on glories. *Appl. Opt.*, **47**, H133–H142, doi:10.1364/AO.47.00H133.
- , 2008b: Noncircular glories and their relationship to cloud droplet size. *Appl. Opt.*, **47**, H25–H30, doi:10.1364/AO.47.000H25.
- , 2015: Re-visiting the atmospheric corona. *Appl. Opt.*, **54**, B46–B53, doi:10.1364/AO.54.000B46.
- Lee, R. L., and P. Laven, 2011: Visibility of natural tertiary rainbows. *Appl. Opt.*, **50**, F152–F161, doi:10.1364/AO.50.00F152.
- Lefaudeux, N. A., 2011: Crystals of hexagonal ice with (2 0 -2 3) Miller index faces explain exotic arcs in the Lascar halo display. *Appl. Opt.*, **50**, F121–F128, doi:10.1364/AO.50.00F121.
- Markiewicz, W. J., and Coauthors, 2014: Glory on Venus cloud tops and the unknown UV absorber. *Icarus*, **234**, 200–203, doi:10.1016/j.icarus.2014.01.030.
- Minnaert, M. G. M., 1993: *Light and Color in the Outdoors*. Springer-Verlag, 417 pp.
- Möbius, W., 1910: Zur Theorie des Regenbogens und ihrer experimentellen Prüfung. *Ann. Phys.*, **338**, 1493–1558, doi:10.1002/andp.19103381622.
- Parviainen, P., C. F. Bohren, and V. Mäkelä, 1994: Vertical elliptical coronas caused by pollen. *Appl. Opt.*, **33**, 4548–4551, doi:10.1364/AO.33.004548.
- Petrova, E. V., S. Oksana, W. J. Shalygina, and W. J. Markiewicz, 2015: The VMC/VEx photometry at small phase angles: Glory and the physical properties of particles in the upper cloud layer of Venus. *Planet. Space Sci.*, **113–114**, 120–134, doi:10.1016/j.pss.2014.11.013.
- Riikonen, M., M. Sillanpää, L. Virta, D. Sullivan, J. Moilanen, and I. Luukkonen, 2000: Halo observations provide evidence of airborne cubic ice in the Earth's atmosphere. *Appl. Opt.*, **39**, 6080–6085, doi:10.1364/AO.39.006080.
- Shaw, J. A., R. L. Lee, and P. Laven, 2015: Light and color in the open air: Introduction to the feature issue. *Appl. Opt.*, **54**, LC1–LC2, doi:10.1364/AO.54.000LC1.
- Tape, W., 1994: *Atmospheric Halos*. Antarctic Research Series, Vol. 64, Amer. Geophys. Union, 143 pp.
- , and J. Moilanen, 2006: *Atmospheric Halos and the Search for Angle X*. Amer. Geophys. Union, 238 pp., doi:10.1029/SP058.
- Theusner, M., 2011: Photographic observation of a natural fourth-order rainbow. *Appl. Opt.*, **50**, F129–F133, doi:10.1364/AO.50.00F129.
- Tomasko, M. G., and Coauthors, 2005: Rain, winds and haze during the Huygens probe's descent to Titan's surface. *Nature*, **438**, 765–778, doi:10.1038/nature04126.
- Tränkle, E., and B. Mielke, 1994: Simulation and analysis of pollen coronas. *Appl. Opt.*, **33**, 4552–4562, doi:10.1364/AO.33.004552.
- Van de Hulst, H. C., 1947: A theory of the anti-coronae. *J. Opt. Soc. Amer.*, **37**, 16–22, doi:10.1364/JOSA.37.000016.
- Venturi, G. B., 1814: *Commentari sopra la storia e la teorie dell'Ottica*. Pe' Fratelly Masi, 246 pp. [Available online at [www.e-rara.ch/zut/content/titleinfo/2654827](http://www.e-rara.ch/zut/content/titleinfo/2654827).]